JOURNAL OF MATERIALS SCIENCE **39** (2004) 787–801

Electrophoretic deposition—mechanisms, myths and materials

Y. FUKADA, N. NAGARAJAN, W. MEKKY, Y. BAO, H.-S. KIM, P. S. NICHOLSON
Ceramic Engineering Research Group, Department of Materials Science and Engineering, McMaster University, 1280 Main Street West, Hamilton, Ontario L8S 4L7, Canada
E-mail: fukaday@mcmaster.ca

Explanations of the deposition process during electrophoretic deposition (EPD) are presented and their boundary conditions discussed. It is suggested increasing resistance during EPD is due to the deposit and not dilution of current carrying species in the suspension. Dialysis membrane experiments demonstrate ions carry significant current. Side-effects of two suspension-conditioning agents are described, i.e., TMAH and PEI. The former can induce "aging" in suspension as its surface adsorption varies with time and reduces suspension pH. PEI appears to adsorb on all ceramic and metal powders, so may be a universal EPD agent for stoichiometric deposition of ceramic/ceramic and ceramic/metal powder-mixtures. Novel structures produced by EPD are presented.

1. Introduction

Electrophoretic deposition (EPD) is a colloidal process wherein materials are shaped directly from a stable suspension by a dc electric field. EPD involves two processes, one well understood (electrophoresis) [1, 2] and one less so (deposition). This paper discusses aspects of the latter and some questions raised in the literature thereabout.

2. Mechanism of deposit formation during EPD

The mechanism of deposition during EPD has been the subject of much study. Although mechanisms have been proposed to explain experimental results, a full understanding is lacking. As Van der Biest and Vanderperre note [3], although EPD has been used successfully without a clear picture of the mechanism, a better understanding is needed to decrease the work to determine optimum conditions.

As per Zhitomirsky's analysis [4], the proposed mechanisms can be divided into three categories, i.e., (a) charge-neutralisation or electrocoagulation, (b) zeta-potential lowering, or electrochemical coagulation, and (c) particle accumulation.

2.1. Particle charge neutralisation

Grillion *et al.* [5] suggested particles suffer charge neutralisation as they touch the electrode (or deposit) and become static. This mechanism is important for single particles and monolayer deposits. It explains deposition of powders that charge on salt addition to the suspension; e.g., the deposition of aluminium (Brown and Salt [6]). This mechanism explains initial stage deposition from very dilute suspensions but is invalid under the following conditions.: (a) EPD for longer times (thick deposits), (b) when particle-electrode processes are prevented, e.g., a semi-permeable membrane induces deposition between the electrodes, and (c) when reactions occur at the electrode which alter the pH thereabout.

2.2. Electrochemical coagulation of particles

This mechanism implies reduction of the repulsive forces between particles. Coagulation due to increase of electrolyte concentration around the particles was discussed by Koelmans [7]. He proposed the increase in electrolyte concentration near the depositing electrode lowers the zeta potential and induces flocculation. This mechanism is plausible when electrode reactions generate OH^-, e.g., suspensions containing water. Zhitomirsky [4] lists the cathodic reactions that involve the generation of OH^- ions. This mechanism is invalid when there is no increase of electrolyte concentration near the electrode. For the latter, Sarkar and Nicholson [8] offered an explanation. Consider a positively charged oxide particle/lyosphere system moving towards the cathode in an EPD cell. Fluid dynamics and the applied electric field will distort the double layer envelope, thinner ahead, and wider behind, the particle. The counterions in the extended tail can react with the cations also coming to the cathode and reduce the thickness of the double-layer. The next incoming particle with the thin, leading-edge double layer can now approach close enough for London Van der Waal attractive forces to dominate and induce coagulation/deposition. This mechanism is shown in Fig. 1. The distortion of the double layer leading to coagulation is plausible considering the high concentration of particles near the electrode (or high collision frequency).

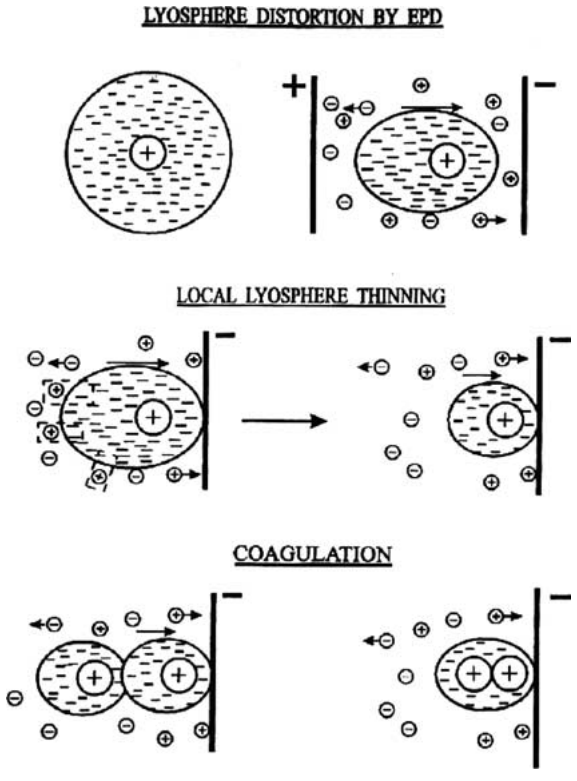

Figure 1 Schematic of the deposition mechanism by lysophere distortion and thinning [8].

Secondly, this mechanism works for incoming particles with thin double layer heads, coagulating with particles already in the deposit. One postulate not applicable to EPD is, that cations are in excess near the cathode. De and Nicholson [9] showed that, contrary to the Sarkar-Nicholson postulate, H^+ are depleted by discharge at the cathode. They suggest this increases the local pH towards the isoelectric point (pH_{iep}), which facilitates coagulation. The discharge of H^+ occurs vis:

$$H^+_{x=\infty} \overset{\text{transport-process}}{\rightarrow} H^+_{x=0} + e^- \overset{\text{charge-transfer}}{\rightarrow} \frac{1}{2}H_2 \quad (1)$$

When charge transfer at the electrode consumes H^+, the $[H^+]$ at the electrode/solution interface drops below the bulk value, creating a concentration gradient thereof. The concentration of H^+as a function of distance and time is obtained by solving the classical diffusion equation with boundary conditions:

$$\text{(a)} \quad C = C_{\text{bulk}} \text{ (at } x = \infty) \quad (2a)$$

$$\text{(b)} \quad (j_{c,\text{total}})_{x=0} = -D_{\text{eff}} \left(\frac{\partial C}{\partial x}\right)_{x=0} = \lambda = \frac{I}{Z_c F} \text{ (at } x = 0) \quad (2b)$$

where I is the current density, λ a constant, j the flux and $D_{\text{eff}} = D_c D_a (Z_a + Z_c)/(Z_c D_c + Z_a D_a)$ (sub 'c' = cations: sub 'a' = anions: Z = valencies).

The solution is:

$$C = C_{\text{bulk}} - \frac{\lambda}{D_{\text{eff}}^{0.5}}\left[2\left(\frac{t}{\pi}\right)^{0.5} \exp\left(-\frac{x^2}{4D_{\text{eff}}t}\right) - \frac{x}{D_{\text{eff}}^{0.5}}\left\{1 - \text{erf}\left(\frac{x^2}{4D_{\text{eff}}t}\right)^{0.5}\right\}\right] \quad (3)$$

which is used to determine $C = f(x, t)$, since all other parameters are known. De and Nicholson's results for the concentration and pH of an alumina/EtOH suspension as a function of time, are shown in Figs 2a and b. As steady state with respect to diffusion and charge transfer of H^+ ions is approached, the pH adjacent the electrode approaches a value of 7, the isoelectric point of alumina. So, as these particles move to the cathode, their zeta-potential reduces due to increasing pH. When $pH \approx pH_{iep}$, the particles coagulate. This mechanism is universal for suspensions involving H^+ (or H_3O^+).

2.3. Flocculation by particle accumulation

Hamaker and Verwey [10] suggested EPD is akin to sedimentation and the primary function of the applied field is to move the particles towards the electrode. Accumulated particles then deposit due to the pressure exerted by those incoming and in the outer layers. This mechanism is feasible when deposition does not occur at the electrode, e.g., deposition on a dialysis membrane (Sarkar and Nicholson [8]). It explains

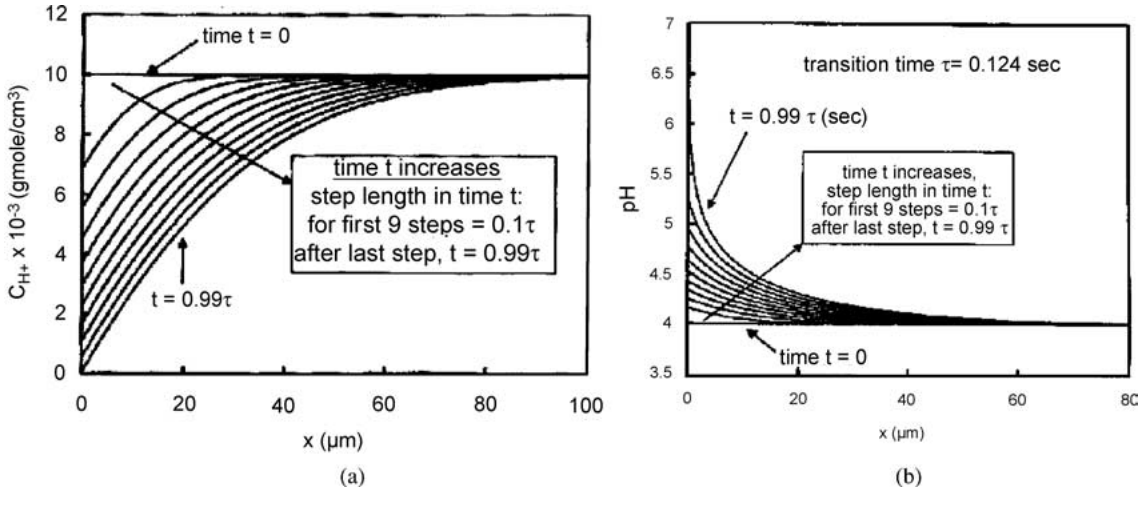

Figure 2 (a) Profile of co-ion (H^+) concentration as function of time 't' and distance 'x'. (b) Profile of suspension pH as a function of time 't' and distance 'x' [9].

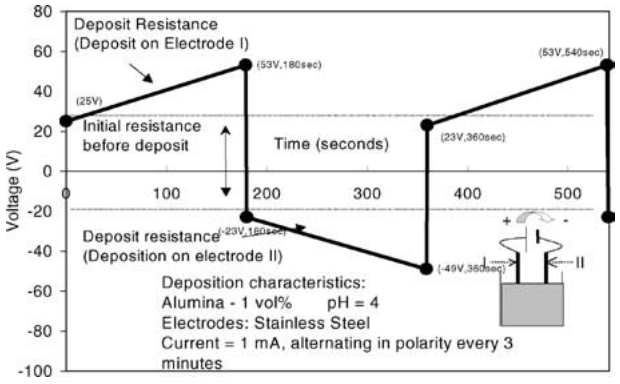

Figure 3 Deposition voltage as a function of time, with a DC field alternating in polarity every 180 s.

deposits on porous membranes that are not electrodes. Vanderperre [11] noted that, when the solids loading is increased, the zeta potential of the particles shifts towards the isoelectric point. This observation supports this mechanism.

3. Myths about EPD

3.1. The source of increasing resistance in the EPD cell

Van der Biest and Vanderperre [3] consider the total resistance of the EPD cell increases via depletion of charge carriers from the suspension.

The present authors electrophoretically deposited an alumina suspension, switching the polarity of the electrodes every three minutes (Fig. 3). The initial voltage (25 V) betrays the suspension resistance plus the resistance due to the deposit layer formed at the initial instant of current passage. The deposit voltage increases to 53 V in 180 s. The polarity was then changed and the resistance dropped to $\cong$25 V (negative due to change of current direction). The voltage again increased to 53 V in three minutes and the same result was obtained on changing polarity again. This indicates the suspension conductivity remains constant, i.e., the voltage returns to the same value each time the polarity is changed, i.e., the ohmic drop is due to the deposit. These observations argue against the mechanism proposed by Van der Biest and Vandeperre [3].

3.2. What carries the current in the suspension: ions or particles?

Sarkar and Nicholson [8] inserted a dialysis membrane between the EPD electrodes in an Al_2O_3 suspension. The membrane is permeable to ions but a dense deposit formed thereon and current passed via ionic discharge at the cathode. They concluded the majority charge is carried by ions and current passage results therefrom.

Zhang and Lee [13] found the current drops dramatically when an insulating polymer film is inserted perpendicular to the electric field between the electrodes. This drop was not observed when the film was placed parallel to the electric field. They suggest, the current drop is due to blockage of particle movement and not by an increase of suspension resistance due to the polymer film. Thus, they conclude the primary charge carriers are the charged particles. They ignored the fact that charged ions in the suspension are also motion-prohibited by the film. Thus the particles are identified, but no rationale is given for the prohibition of ionic motion.

Moreno and Ferrari [14] reported the deposited mass per unit area (m) is proportional to ζ/s (ζ = zeta-potential, s = conductivity) if the concentration of particles in suspension (C), electric current (I) and deposit time (t), are fixed. Their model suggests the sticking probability of particles on particles-at-the-substrate, is unity, suggesting the suspension conductivity is the parameter to control EPD. Even if the alumina has a high enough zeta-potential to deposit, the electrophoretic-deposition-rate and deposition-probability must decrease with increasing suspension conductivity. Again, it is assumed the particles are the majority current carriers, and the ions in the system are ignored. Sticking factors are considered later.

Tang *et al.* [15] measured deposit weight from a 3 vol% γ-Al_2O_3 suspension as a function of time, at various values of pH. Maximum weight was obtained at pH = 8, a value close to the isoelectric point (pH = 9.6). They observed minor deposition at pH = 4 though the zeta-potential is maximum thereat. They used hydrochloric acid to produce low pH values. This results in increased $[H^+]$ and $[Cl^-]$, i.e., higher suspension conductivity. It is probable H^+ is the dominant current carrier and the transport number of the γ-Al_2O_3 particles is reduced thereby. The minor deposit at pH4, though the suspension is well dispersed, led them to conclude the charge carriers are protons.

Uchikoshi *et al.* [16] measured the transport number for Al_2O_3 particles and the amount of deposit, in various solvents at differing pH values. They found the transport number for Al_2O_3 particles in H_2O is $<1\%$ at the maximum deposition rate. This value further decreases with increasing $[H^+]$, i.e., the charge carriers are H^+ and not the charged particles.

3.3. Does the electrode influence the nature of the deposit?

Aldykiewicz *et al.* [17] studied the deposition of cerium-rich films on copper under cathodic polarization. They found the cathodic polarization of Cu in aerated solution containing cerium ions yields a tetravalent cerium-rich film that blocks the oxygen reduction reaction and prevents the corrosion of Cu.

Uchikoshi *et al.* [18] compared four different EPD electrodes to deposit Al_2O_3 from H_2O, i.e., platinum, palladium, nickel and stainless steel. Their aim was to produce bubble-free deposits from an aqueous suspension as palladium absorbs hydrogen.

The present authors measured the deposition rate on four cathodes, i.e., stainless steel, copper, palladium and graphite (Fig. 4). The highest deposition rate was obtained on copper, however, after removing the deposit, there was evidence of reaction therebetween, i.e., the corrosion reaction mentioned by Aldykiewicz *et al.* [17]. It was found that, adding 0.1 wt% water to the EtOH, reduced the deposition rate on palladium. It is suggested hydrogen adsorption therein rate-controls the deposition process (Fig. 5).

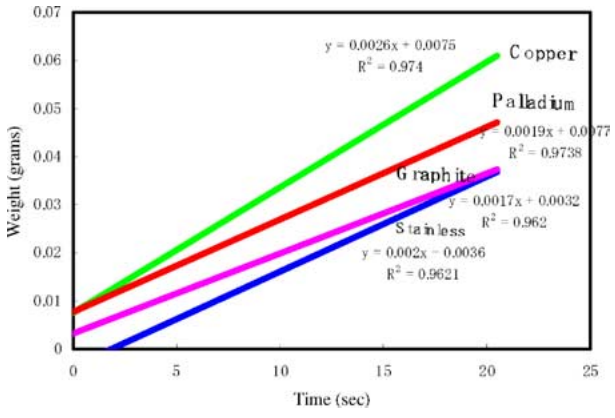

Figure 4 Electrophoretic deposition for different electrodes.

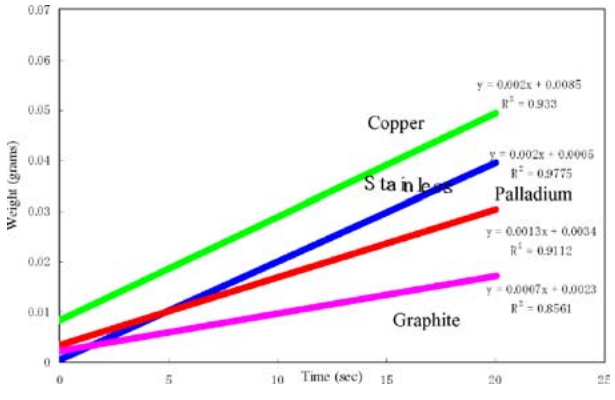

Figure 5 Electrophoretic deposition for different electrodes, 1 vol% water in ethanol.

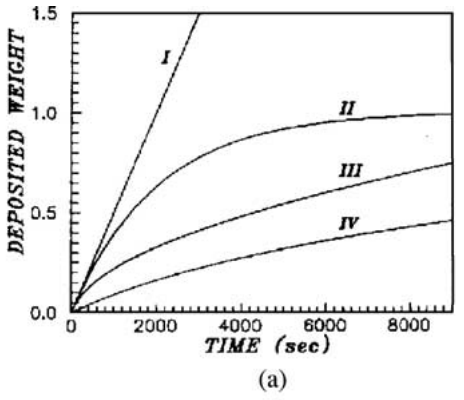

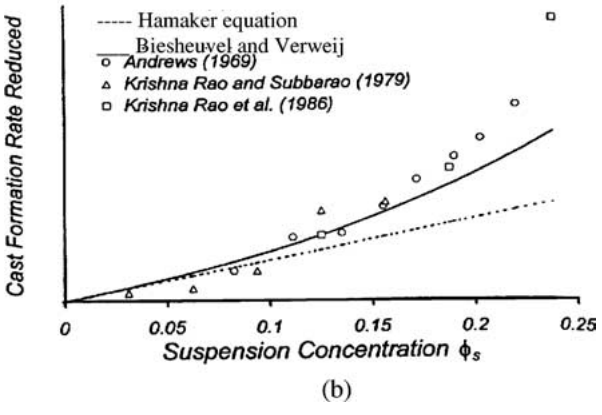

Figure 6 (a) Schematic of deposited weight fraction as a function of time for four different conditions (curve I, constant current/constant concentration: curve II, constant current/variable concentration: curve III, constant voltage/constant concentration: and curve IV, constant voltage/variable concentration). (b) Cast formation rate as a function of suspension concentration. Comparison of data from various authors (provided by Biesheuvel and Verwweij) [19].

3.4. The non linearity of deposition rates from concentrated suspensions

Deviation from linearity of deposition rates has been studied under constant current and constant voltage, EPD. The non-linearity for dilute suspensions is due to concentration depletion. In addition, in constant voltage EPD, the non-linear deposition rate is also due to the higher deposit resistivity [8]. The latter causes the voltage drop/unit length of the suspension to decrease with time (Fig. 6a).

Recently, Biesheuvel *et al.* [19] derived a rate equation for cast formation during electrophoretic deposition (EPD). They attempted to explain the greater-than-linear rate of cast formation with increasing suspension concentration during EPD, via a new rate equation:

$$Y = -\mu E S c_c \frac{\phi_s}{\phi_c - \phi_s} t \tag{4}$$

where Y is the yield, μ, the electrophoretic mobility, E, the local field strength, S, the electrode surface area, c_c, the cast mass concentration, ϕ_s, the suspension volumetric concentration, ϕ_c, the cast volumetric concentration and t is the time of deposition.

Their analysis involve two assumptions, (a) particle charge can be ignored whilst calculating the electric field strength from the Poisson equation, and (b), the diffusion flux of particles is negligible.

The assumption that particle charge can be ignored while calculating the electric field strength infers the particles have no surface charge or double layer i.e., they have no ζ-potential (or $\zeta = 0$). This implies their electrophoretic mobility 'μ' is zero. If $\zeta = 0$, the particle velocity, 'v', will be zero (if $\mu = 0$). Thus, the particles (uncharged) will not move under an impressed electrical field so no electrophoretic deposition will occur!

The authors used the continuity equation to prove the volumetric concentration of particles in the suspension, 'φ_s', is independent of their location (r) in the suspension phase and of time (t). The reasoning thereof is fallacious. The continuity equation used is:

$$\frac{\partial \varphi_s}{\partial r} = -\frac{1}{r^\sigma}\frac{\partial}{\partial r}(r^\sigma J). \tag{5}$$

Now, the total flux, J_{total}, will be the sum of two contributions;

$$J_{\text{total}} = J_{\text{electric field}} + J_{\text{diffusion}} \tag{6}$$

where $J_{\text{diffusion}}$ and $J_{\text{electric field}}$ are contributions to the total flux (J_{total}) by diffusion and electric field respectively. The authors ignored the diffusion flux in the continuity Equation 6 reasoning that, "Ordinary diffusion as a means of particle transport in the suspension phase has been omitted, because gradients $\partial\varphi_s/\partial r$ do not develop in the suspension phase, as explained later. . . ."

However, their explanation is based on the assumption that the diffusion flux, $J_{\text{diffusion}} = -D\partial\varphi_s/\partial r$ is equal to zero in the continuity Equation 5. They suggest this is valid for all time (D is the diffusion coefficient). This argument is circular and therefore fallacious.

The cast-formation-rate Equation 4 deviates from experiment at high suspension concentrations (Fig. 6b). The authors explain that the (cast) structure becomes more porous as the suspension concentrates. This 'crowding effect' leads to particle interference, which prevents particulate settling into a dense network. Thus they explain the higher experimentally-observed cast formation rate, as porous casts are associated with lower φ_c values. However, if the crowding of particles leads to particle interference, their analysis is bound to give erroneous results because all particles are assumed to have a constant velocity with time (t) and position (r) i.e., they are assumed to move independently!

3.5. Is the "sticking-factor," quantifyable?

The sticking factor compares the deposition rates of powders under various conditions [20, 21]. Estimates are approximate, i.e., uncertainties enter the calculations. An estimate is obtained from the Hamaker and Hückel equations. The Hamaker equation is:

$$m = \alpha C v S t \tag{7}$$

where m is the mass of deposit, α the sticking factor, C the concentration of particles, v the velocity of the particle, S the electrode surface area and t the time of deposition. The velocity of a particle, 'v', is calculated from the Hückel equation:

$$v = 2E\varepsilon_r\varepsilon_0\zeta/3\eta \tag{8}$$

where, E is the electric field, ε_r the dielectric constant of the dispersion, ε_0 the permittivity of free space, ζ the zeta potential and η the viscosity of the medium. The important experimental quantities are (1) the electric field, (2) the viscosity, (3) the dielectric constant, and (4) the zeta-potential. Errors in the first three are likely large, so calculation of the sticking factor using the Hamaker and Hückel equations is meaningless. In the EPD of non-conducting particles, the resistance of the deposit is the major contribution to the cell resistance, which infers most of the voltage-drop occurs within the deposit, so the assumption of an average value of E is incorrect. The dielectric constant and viscosity of the suspension are also different near the electrode, as different conditions exist thereat vis à vis the bulk. Thus, assuming constant values of solvent-dielectric-constant and solvent-viscosity lead to calculation errors.

4. The surface chemistry of EtOH suspensions for EPD

EPD is a facile process for fabrication of ceramic monoliths, composites, laminates and functionally graded materials. EPD from aqueous suspensions has the disadvantage of water-electrolysis at low potentials (2 V/cm) [8]. So, non-aqueous solvents are considered, e.g., EtOH.

4.1. Ionically-stabilised, EtOH suspensions

Wang *et al.* [22] and Wang and Nicholson [23–25] proved alumina particles in ethanol are charged-stabilized, the mechanism being the adsorption of protons or hydroxyl ions onto the hydroxylated alumina surface. The 'acidity' (pH) of ethanol suspensions was determined via the ion-transfer function and called the "operational pH". The surface charge on the Al_2O_3 changed from positive to negative as the operational pH increased. They concluded the total interaction energy of Al_2O_3 in EtOH can be calculated using DLVO theory. The resulting calculations suggest that particle interactions can be dominated by ionic repulsion via control of the electrolyte concentration. Fukada and Nicholson [26] explored the stability of non-oxide ceramic powders, i.e., Si_3N_4, SiC and $MoSi_2$ in ethanol. They compared their results to the behaviour of SiO_2 in ethanol. The isoelectric point of $MoSi_2$ (2.2) was more acidic than Si_3N_4 (9.0) or SiC (5.4) as the surface oxide was thicker and involved MoO_3. Increasing the thickness of oxide on the surface shifts the isoelectric point to lower pH values. The basic amine surface groups on Si_3N_4 shift the isoelectric point to higher pH values, though the oxide layer is similar to that on SiC in ethanol. They also concluded DLVO theory defines the stability of Si_3N_4, SiC and $MoSi_2$ in EtOH.

The Stability Ratio (W) is often used to quantify suspension stability [27]. W is the ratio of rate-of-rapid-coagulation (J_R) to slow-coagulation (J_S), i.e.,

$$W = \frac{J_R}{J_s} = 2a\int_{2a}^{\infty}\exp\left(\frac{E(D)}{kT}\right)D^{-2}\mathrm{d}D \tag{9}$$

Wang *et al.* [24] calculated W for an alumina-ethanol suspension. Their results, (Fig. 7a and b), suggest W is closely related to the zeta potential. Fukada and Nicholson [26] determined this correlation for non-oxide suspensions i.e., Si_3N_4, SiC, and $MoSi_2$/EtOH suspensions (Fig. 8a and b). They concluded the stability ratio data supports the DLVO results.

4.2. Non-oxide powder suspensions in EtOH: aging effects

EPD requires a stable suspension thus if surface-chemistry changes with time, i.e., "aging", it must be examined. Bergström and Bostedt [28] and Laarz *et al.* [29] reported the aging effect of Si_3N_4 in an aqueous medium. Si_3N_4 undergoes hydrolysis and dissolution in water which causes the aging. Van der Biest and Vandeperre [3] suggest the changes of pH upon addition of a powder to water has received little attention. The pH of such suspensions can change substantially and unpredictably. They point out the natural pH of a suspension tends towards the point-of-zero-charge (pzc) of the powder (Fig. 9). Windergren and Bergström [30] examined Al_2O_3, TiO_2 and SiC in EtOH with four different additives, i.e., Acetic acid (HAc), Citric acid,

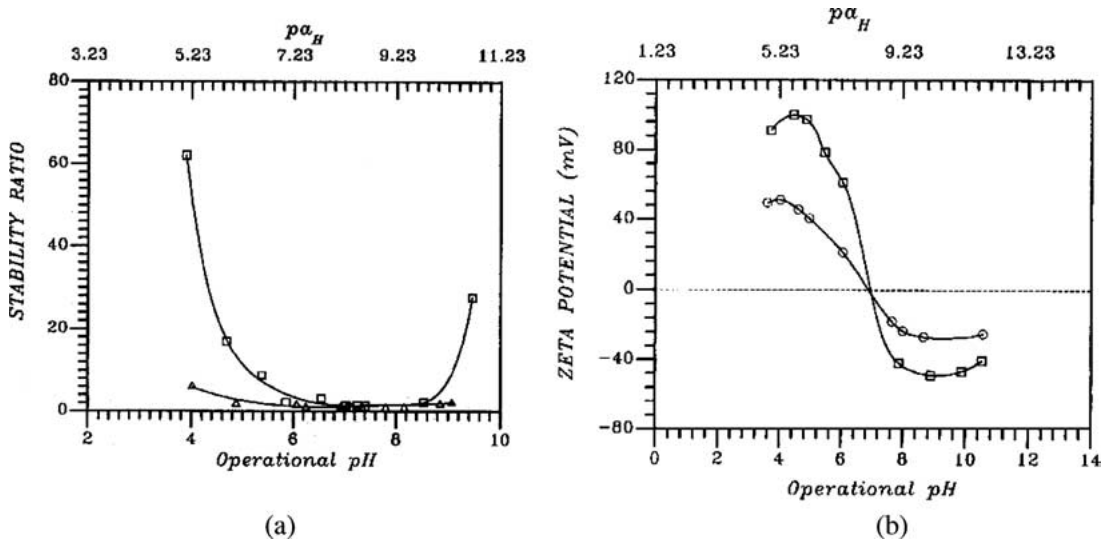

Figure 7 (a) Stability ratio (W) as a function of the alumina-EtOH suspension pH and pa_H ((□) EtOH and (Δ) EtOH (10^{-3} M LiCl)). (b) Zeta potential of alumina in ethanol as a function of the suspension pH and pa_H ((□) EtOH and (O) EtOH (10^{-3} M LiCl)).

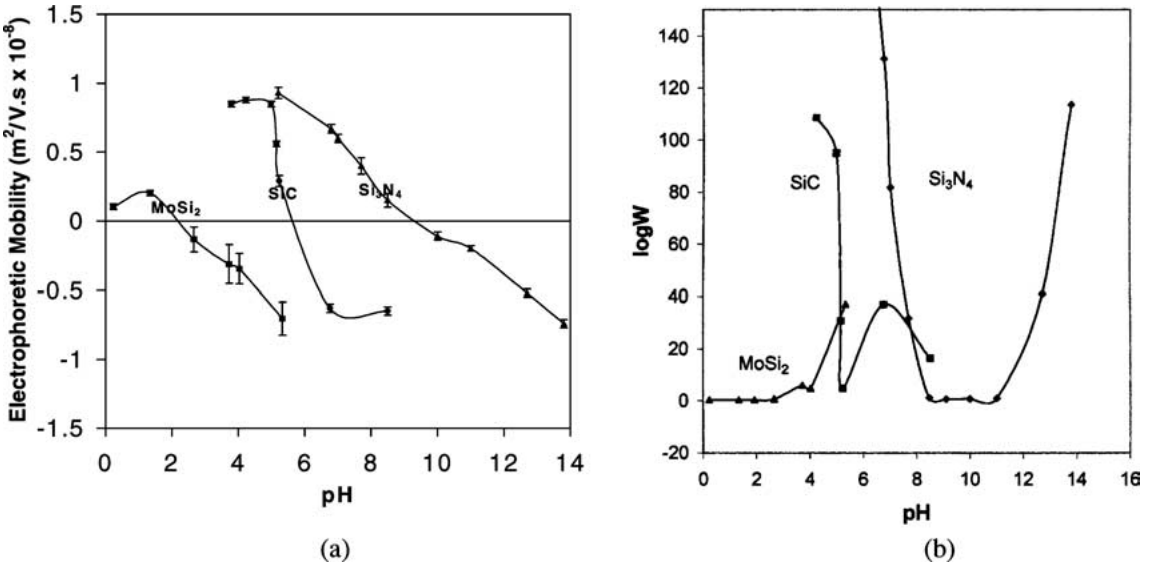

Figure 8 (a) Electrophoretic mobility versus pH for Si_3N_4, $MoSi_2$ and SiC in ethanol. (b) Stability ration versus pH for Si_3N_4, $MoSi_2$ and SiC in ethanol.

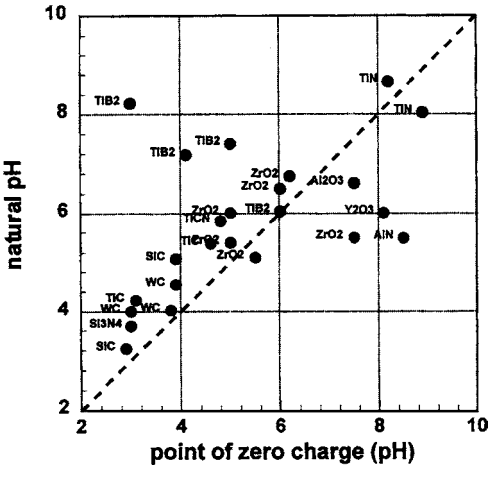

Figure 9 The natural pH of a range of commercially available powders, for a powder loading of 20 gL^{-1}, as a function of their point-of-zero-charge n water. In general, the natural pH indeed tends to be close to the point of zero charge. Deviations observed can be attributed to the presence of adsorbed acids or bases [3].

HCl, LiOH and Triethanolamine (TEA). They found that none of the additives provided long-time stability to SiC via settling studies, i.e. suspensions were unstable and settled in minutes. TEA (base) stabilized both Al_2O_3 and TiO_2 so, they suggested TEA specifically adsorbs at the oxide/liquid interface.

Fukada and Nicholson [31] investigated the aging effect of non-oxide ceramic powders dispersed in ethanol. The dissolution of CO_2 in the suspension could change the acidity during measurement so dry nitrogen gas was flowed through ascarite to adsorb CO_2. The pH change versus time for the SiC/EtOH system under dry nitrogen is shown in Fig. 10. The pH of the basic suspension decreases with time. The curve for pure EtOH (Curve 1) is also plotted as reference. pH drops with time for Curve 3 (premixed EtOH + SiC) but most dramatic is when SiC is added to pure EtOH (Curve 2). The pH immediately decreases from 10.1 to 8.2, demonstrating the powder-surface influence on the suspension pH. Si_3N_4/EtOH showed the same tendency. The basic pH

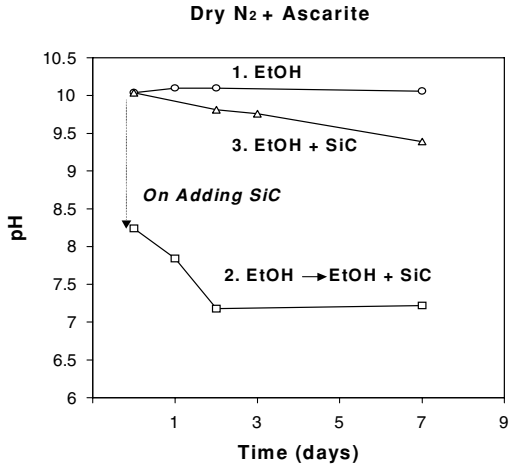

Figure 10 The pH change versus time for the Si_3N_4-EtOH system under dry N_2 atmosphere.

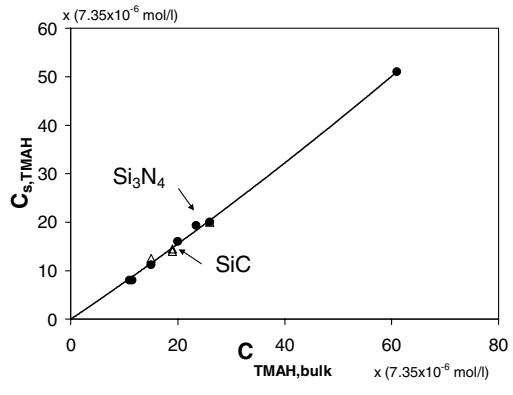

Figure 11 Adsorbed [TMAH] vs. Bulk [TMAH] for Si_3N_4-EtOH and SiC/EtOH.

adjusting-chemical used was tetramethyl ammonium hydroxide (TMAH) and not only does it change the pH but it also adsorbs on the Si_3N_4 and SiC particles. The initial bulk concentration [TMAH], [$C_{TMAH,bulk}$], and adsorbed surface concentration [TMAH], [$C_{s,\ TMAH}$], were obtained by measuring the EtOH pH before adding the powder then remeasuring it after the Si_3N_4 (or SiC) were added to the EtOH (supernatant pH measured). The data plotted in Fig. 11 were estimated from the calibration curve so only show qualitative information. The pH drop is due to physiochemical adsorption of TMAH and the consequent removal of OH^- from the liquid. The latter drives the suspension pH acidic and results in suspension instability (Fig. 11). The addition of $MoSi_2$ powder to EtOH/TMAH dropped the pH from 10.3 to 5.6 (Fig. 12). This drop is more than induceable by the TMAH addition so another effect must be in play. $MoSi_2$ powder reacts as an acid in a basic suspension so the latter becomes unstable. To avoid these unwanted changes, Si_3N_4, SiC and $MoSi_2$ should be EPD'd from acidic suspensions of EtOH.

4.3. The EPD of multicomponent suspensions

Suspensions containing particles of more than one type, and/or solvents of more than one type have been

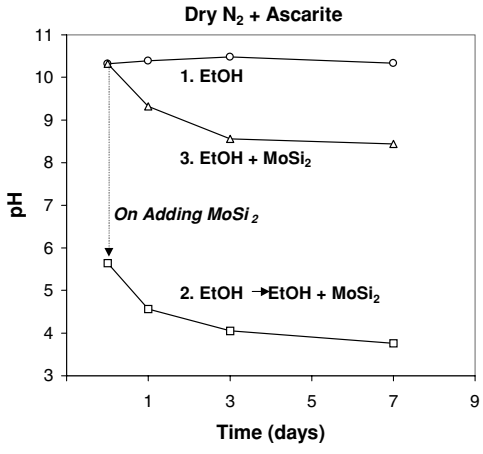

Figure 12 The pH change versus time for the $MoSi_2$-EtOH system under dry N_2 atmosphere.

reported in the literature [32–36], but the properties thereof are poorly understood.

4.3.1. Hetero-coagulation of mixed oxide suspensions for EPD

Hetero-coagulation was first considered by Derjaguin [37], in terms of DLVO theory, later simplified by Hogg *et al.* [38]. In a recent paper, Wang and Nicholson [23] studied hetero-, and homo-, coagulation of alumina-silica and magnesia-silica, suspensions in ethanol. They demonstrated that varying the suspension acidity produces myriad hetero-coagulation architectures. They examined structure formation in binary suspensions by transmission electron microscopy. Fig. 13a shows coagulated alumina-silica particles and Fig. 13b, magnesia-silica particles. Once one phase completely surrounds particles of the other, the mixture EPD's as the former.

4.3.2. Electrophoretic mobility in mixed suspensions and EPD

In mixed-powder, dilute-suspensions, each component moves with its own electrophoretic mobility towards the electrode. The components move with the same mobility at higher concentrations [3]. This is true when concentration depletion of the species is not large and the difference in conductivity of the suspensions is not high. Thus, when components move at their respective mobilities, the mixed particles are interaction free. However, Borner and Herbig [32] reported the calculated mobility (using the additive rule) of polymer-stabilised, mixed, alumina-zirconia powders differs from the experimental mobility. (2 vol% solids dispersed in de-ionised water, with HCl and NaOH used to control pH. The wt% of polymer is assumed with respect to the solids content) (Fig. 14). The difference is highest at low polymer concentrations. Alumina and zirconia particles are oppositely charged in this regime so will hetero-coagulate. When the polymer addition is large, both particles have the same sign and mobility value.

Wang and Nicholson [23] measured the mobilities of alumina-silica and magnesia-silica suspensions in ethanol (Fig. 15a and b). In alumina-silica, the mobility

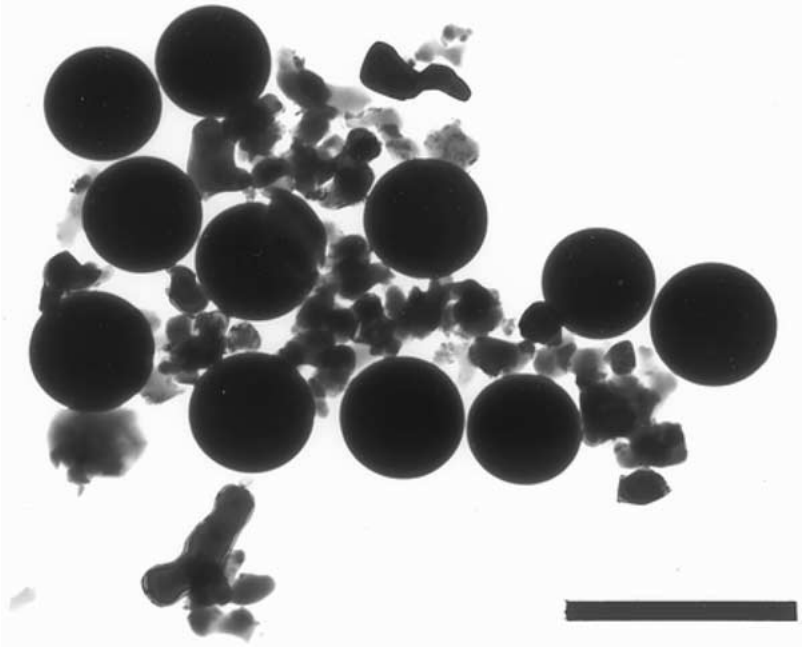

(a)

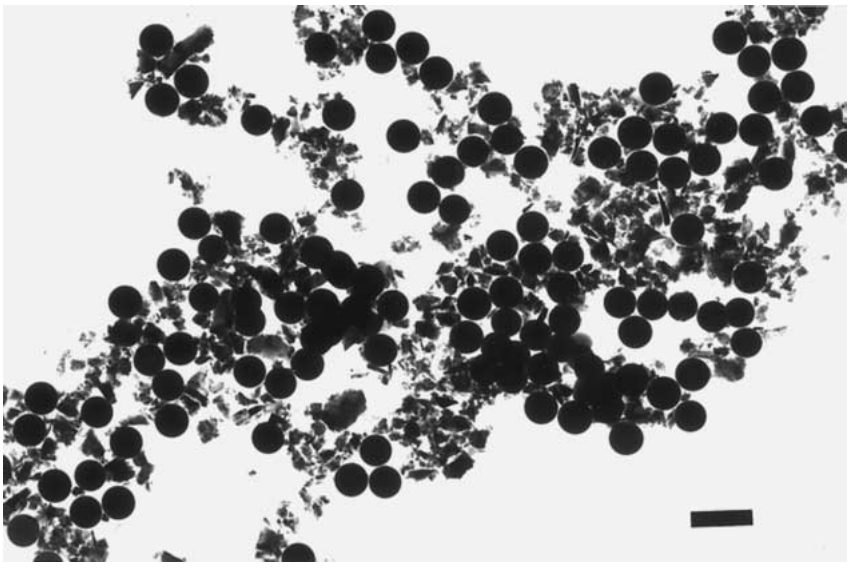

(b)

Figure 13 (a) Micrograph of alumina-silica heterocoagulates at operational pH 6.68 (10 vol% alumina). (b) Micrograph of magnesia-silica hetrocoagulates at operational pH 6.68 (10 vol% magnesia) (bar = 1 μm) [23].

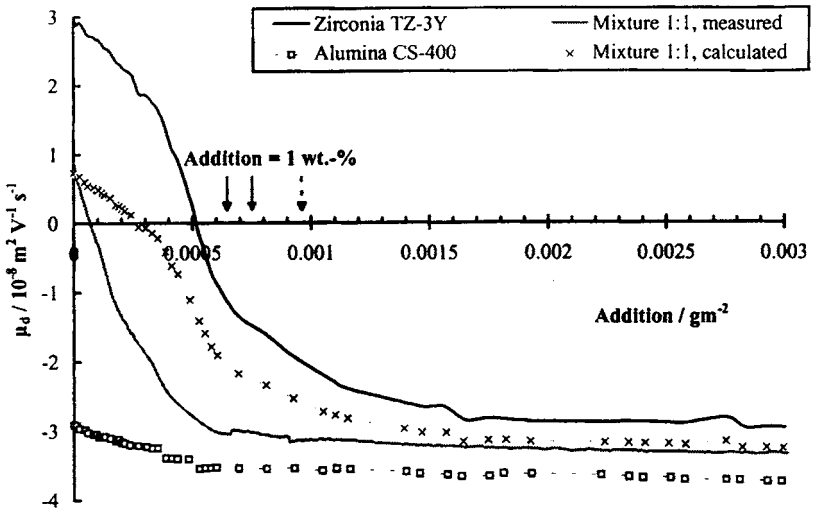

Figure 14 Differences between the calculated and measured mobilities of mixed suspensions [32].

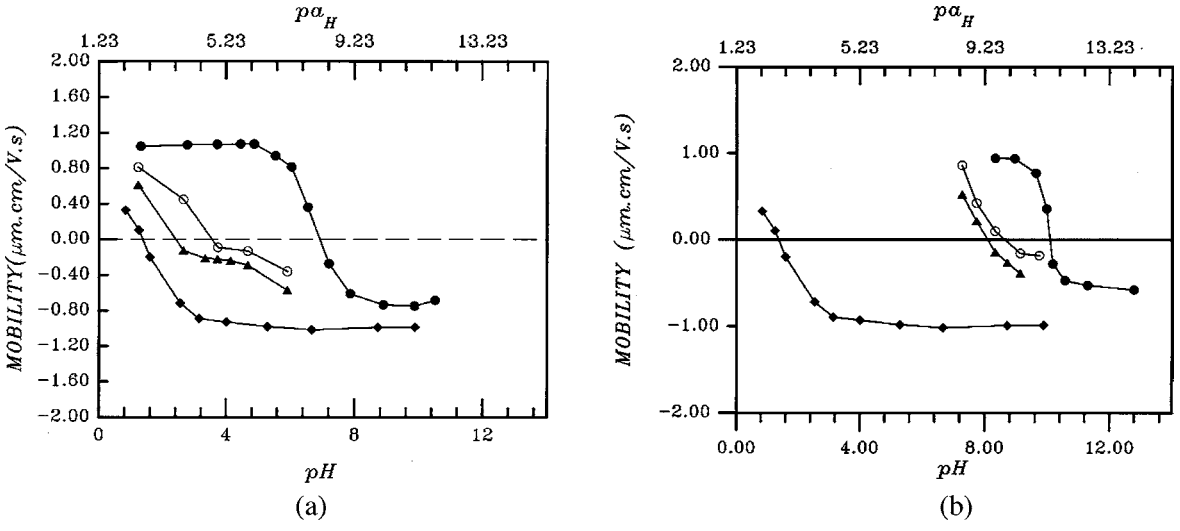

Figure 15 (a) Electrophoretic mobility versus operational pH and pa_H for alumina-silica heterocoagulated particles of various compositions ((♦) silica, (Δ) 5 vol% Al_2O_3, (O) 10 vol% Al_2O_3, (●) Al_2O_3). (b) Electrophoretic mobility versus operational pH and pa_H for MgO-silica heterocoagulated particles of various compositions ((♦) silica, (Δ) 5 vol% MgO, (○) 10 vol% MgO, (●) MgO).

shifts from the negative values for silica to the positive ones for alumina. This is due to hetero-coagulation as the alumina coats the silica and the mobility of the binary particles changes depending on the SiO_2 surface coverage by Al_2O_3. A similar effect was observed for magnesia-silica but the change was more pronounced due to the basicity of even small additions of MgO.

4.3.3. Deposition rates of mixed suspensions during EPD

Borner *et al.* [33] pointed out the particle with the higher mobility will deposit faster at the beginning of the deposition process. However, it also depletes the suspension faster and, due to the dependence of the deposition rate on local concentration, the rate of deposition of the high-mobility component, slows. Yamashita *et al.* [34] observed this effect is prominent at longer deposition times during the deposition of zirconia/hydroxyapatite. They employed mixed solvents (ethanol and acetylacetone), and a mixture of particles. Their simulated results (via the additive rule), agreed reasonably well for <70% acetylacetone (Fig. 16). The discrepancy at higher acetylacetone concentrations is explained by acetylacetone adsorption on zirconia.

The present authors found the deposition rate on a fixed electrode area (gm/sec) is non-linear with composition change for an NiO mixture in ethanol (Fig. 17). At pH = 4, the electrophoretic mobilities are 1.1 μm·cm/Vs (Al_2O_3) and 0.8 μm·cm/Vs (NiO). The observed non-linearity could be due to interaction of particles and conductivity differences between the two suspensions. One way to realise equal mobilities of dissimilar particles is to adsorb the same charged polymer on both.

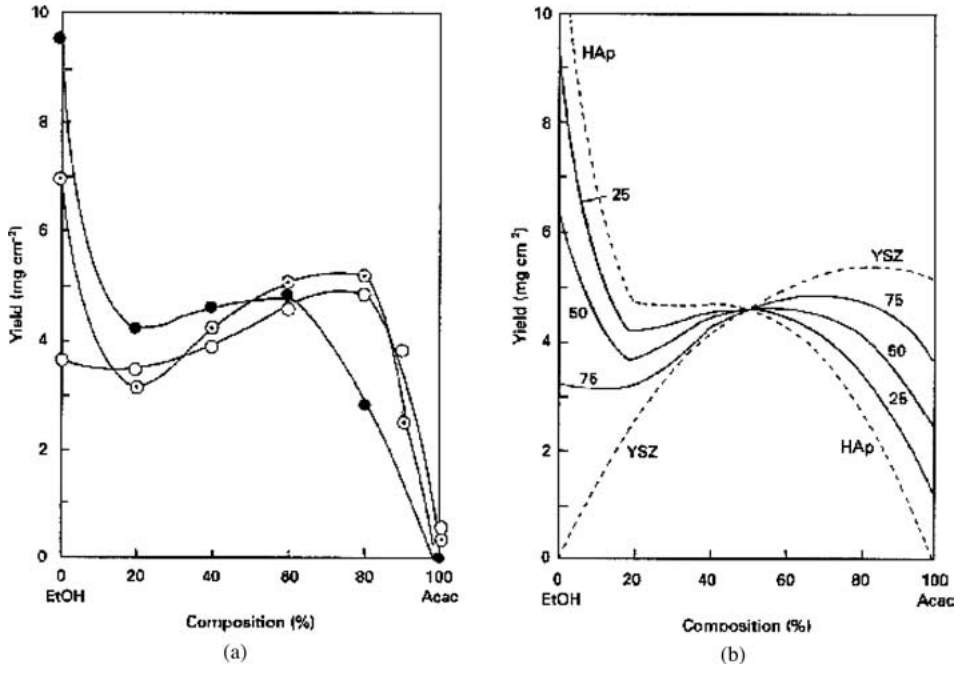

Figure 16 (A) The dependence of deposition yield on the composition ratio of acetylacetone (Acac) to ethanol (EtOH) in the system hydroxyapatite (Hap) and yttria-stabilised zirconia (YSZ). Mixed ratios of YSZ to Hap were (●) 25, (Θ) 50 and (O) 75%. (B) Simulated dependence of yield.

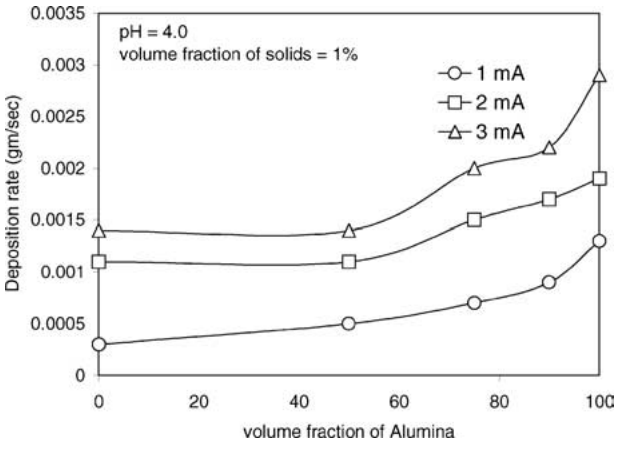

Figure 17 Rate of Deposition of NiO-Al_2O_3 mixed suspensions as a function of alumina volume fraction.

4.4. Polymer-stabilized suspensions in EPD: Is PEI a universal EPD agent?

Sidorov *et al.* [39] and Sindel *et al.* [40] showed that polymers influence the surface charge and mobility of particles.

Dick and Ham [41] observed cationic polyelectrolytes suffer changes of charge on pH and ionic strength alteration. Furthermore, the adsorbability of polyelectolyte on an oppositely-charged surface could change with solution properties. One such polyelectrolyte is polyethylenimine (PEI), a polybase containing primary, secondary and tertiary amine groups in the ratio 1:2:1.

The isoelectric point of silica is ≈pH 2 so, in neutral or basic suspension, it is negatively charged and will deposit on the anode. Hasegawa *et al.* [42] and Dietrich and Neubrand [43] showed this behaviour can be changed by adding PEI, i.e., the surface charge becomes positive for pH < 10.

If particles are soluble in their pH range of deposition (as per ZnO [44] and Y_2O_3 [45]), PEI adsorption renders deposition possible for pH < 10.5. SiO_2 is non-DLVO because a gel layer forms on the surface [46] and ZnO is a semiconductor. Addition of PEI disperses both well and isoelectric points shift to higher pH values.

Thus PEI was explored as a "universal" additive for the EPD of mixtures of metallic and ceramic powders. pH vs. mobility plots for five powders in ethanol are shown in Fig. 18. PEI changes the powder behaviour, magnitude depending on the PEI concentration, [PEI]

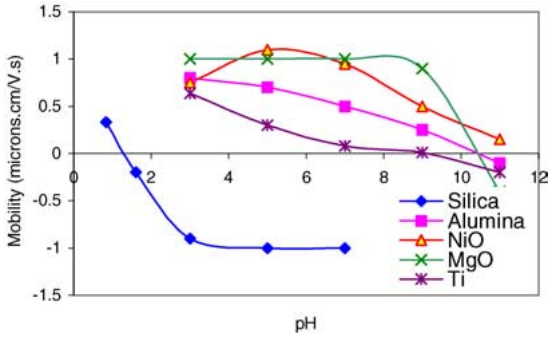

Figure 18 Mobility vs. pH curves for various powders in ethanol.

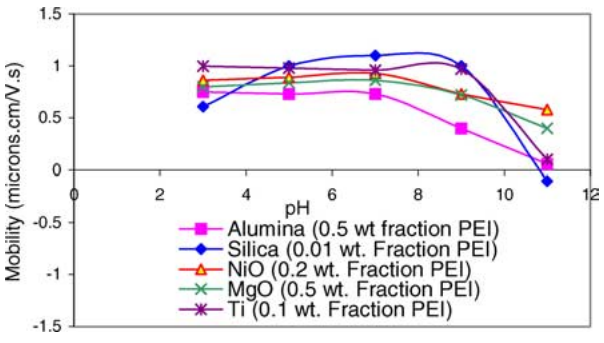

Figure 19 Effect of PEI addition on the mobility of various powders in ethanol.

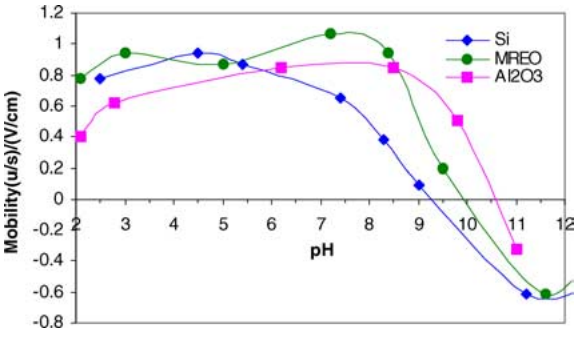

Figure 20 Electrophoretic mobility of Al_2O_3, Si and MREO in ethanol with 1 wt% PEI dispersant.

and the original suspension behaviour. Thus powders can be made behave with similar surface chemistry by individual pre-conditioning with appropriate PEI concentrations before mixing, (Fig. 19).

The electrophoretic mobility of the powder mixture of Si, MREO (mixed rare earth oxide) and Al_2O_3 powders in ethanol with 1 wt% PEI (with respect to the powder) (Molecular weight 10,000) as dispersant, is shown in Fig. 20. All surfaces are positive, pH 3–7.5. Thus a "body" electrophoretically deposited at pH = 7 of α-Al_2O_3, Si and MREO simultaneously deposits. After sintering at 1300°C, the body consists of mullite >90% with minor α-Al_2O_3.

4.5. The EPD of aqueous vs non-aqueous suspensions

Two papers discuss EPD from aqueous vs non-aqueous suspensions, i.e., Van der Biest and Vanderperre [3] and Zhitomirsky [4]. Both suggest EPD from aqueous suspensions is low-cost, low electrical potential and low environmental cost, but hydrogen bubbles are generated by electrolysis of the water. Uchikoshi *et al.* [18] found no macropores in deposits of alumina and zirconia electrophoretic deposited from aqueous suspensions when palladium is used as the EPD cathode. Palladium readily absorbs hydrogen. However use of the aqueous system is restricted as palladium is expensive thus not suited for industrial application.

5. The synthesis of novel materials via EPD

5.1. Micro-laminates

Biological hard tissues, such as mollusk shells, are load-bearing structural materials with lamellar form [47].

They are composed of thick layers of aragonite $CaCO_3$ (ceramic) and thin layers of a protein (organic). Shells exhibit reasonable flexural strength (100–300 MPa) but high fracture toughness (5–11 MPa$\sqrt{m}$). A number of toughening mechanisms co-operate to produce structural flaw tolerance, i.e., interface debonding at lamella boundaries, crack deflection, microcracking, tortuous fracture paths, frictional pull out and energy absorption

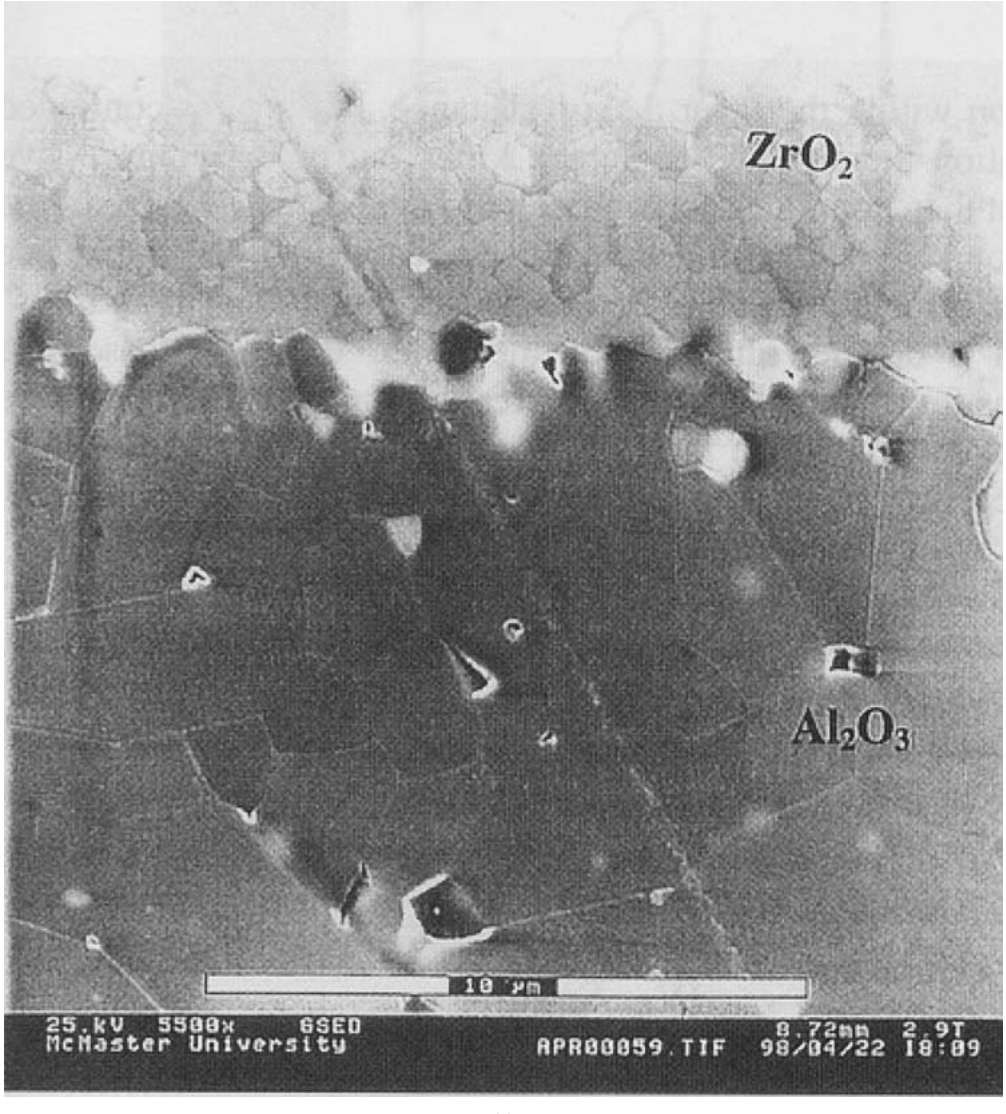

(a)

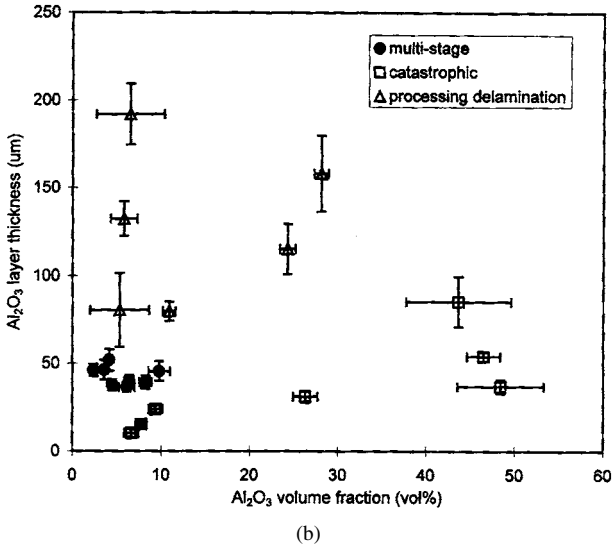

(b)

Figure 21 (a) Dense, well bonded interface of a Al_2O_3/TZ3Y (3 mol% yttria stabilized zirconia) laminate. (b) Map of fracture behavior of all Al_2O_3/TZ3Y composites in terms of Al_2O_3 layer thickness and volume fraction. (c) Change in fracture behavior of an Al_2O_3/TZ3Y laminate with temperature. Left-right temperatures of test are 25°, 400°, 800°, 1000°, 1300°C, respectively [49]. (*Continued*)

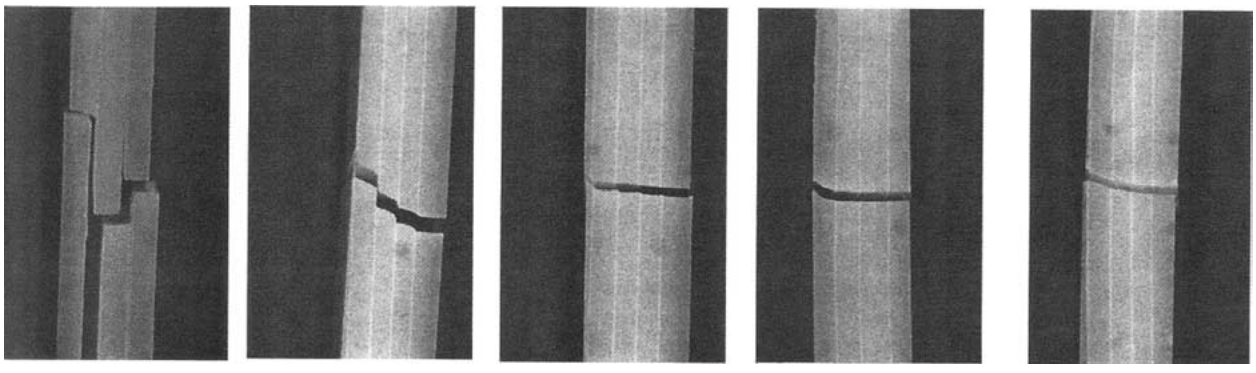

(c)

Figure 21 (*Continued*).

by protein layers. The structure of nature's laminates has been EPD-mimicked in ceramic laminates of thin layers (5–10 μm) of a high compliance material (lanthanum aluminate) in stiff, thicker (20–50 μm) zirconia layers. The advantage of EPD for such laminate synthesis is the large number (100–200) of thin ($\leq$2 μm) layers that can be deposited with interface smoothness of sub micron scale [48].

Laminates with variable layer thickness of ZrO_2 and Al_2O_3 have been produced by Hatton and Nicholson [49] and the fracture behaviour studied with respect to layer thickness, alumina content and temperature. The layers have different Thermal Contraction Coefficients (α) so layer thickness plays a role in crack propagation behaviour due to the compressive stresses generated in layers on cooling from sintering temperatures. The Al_2O_3 layer (lower value of α) suffers compression on cooling. They obtained a dense structure with well-bonded interfaces (Fig. 21a) and mapped the fracture behavior as a function of v/o Al_2O_3 and layer thickness (Fig. 21b). It can be seen from the map that optimum multi-stage fracture conditions occur for alumina layers $\cong$50 μm thick and $<$10 vol% of the total volume. They also showed the parameter $\sigma_r^2 t$ (σ_r = the residual stress in the layer and t = the layer thickness) is a good indicator of the fracture behaviour (stable or unstable) of the laminates. They found fracture behaviour changes with increasing $\sigma_r^2 t$, from catastrophic, to, multi-stage fracture and spontaneous delamination. Fig. 21c illustrates cracking behaviour with changing temperature for an electrophoretically deposited, alumina-zirconia laminate. Step fracture occurs at lower temperatures. As temperature increases, the compressive residual stress in the outer alumina layers, decreases so crack deflection decreases. Hence, for flaw tolerance at high temperatures, a combination of strong and weak layers is required.

5.2. Functionally-graded materials by EPD

Sarkar *et al.* [50] successfully synthesized Al_2O_3/YSZ, $Al_2O_3/MoSi_2$, Al_2O_3/Ni and YSZ/Ni functionally graded materials by constant-current EPD. An alternate fabrication route has been developed for the Al_2O_3/Ni FGMs. Ni powder has a low deposition rate and poor electrode adhesion. It is also dense (8.9 gm/cc) so suffers sedimentation. Thus, an NiO suspension is used and the NiO reduced during sintering. The experimental set-up is shown in Fig. 22. The NiO/EtOH stream is injected (with stirring) into the alumina/EtOH suspension. The "green", FGM is sintered in Ar/ 5% H_2 and the NiO converted to Ni. An SEM micrograph of a cross-section of an Al_2O_3/Ni FGM is shown in Fig. 23.

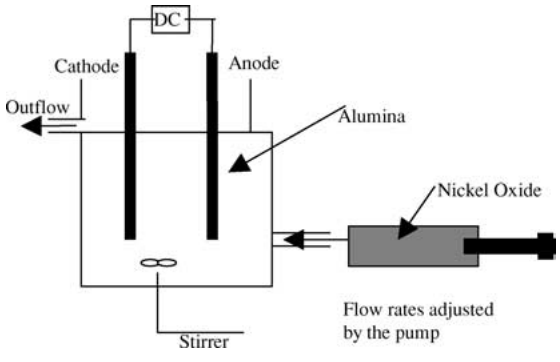

Figure 22 Experimental set up for the synthesis of ceramic/ceramic and ceramic/metal FGMs.

5.3. EPD in a magnetic field

Many materials with non-cubic structure have anisotropic magnetic susceptibility. Under strong magnetic fields, i.e., 10 T, magnetic alignment can occur. Single-crystal, granular α-alumina, (corundum), has a rhombohedral structure and a small anisotropic diamagnetic susceptibility. Uchikoshi *et al.* [51] investigated the texturing of monolithic alumina ceramics by alignment of the Al_2O_3 particles during EPD in a strong magnetic field (10T) (Fig. 24). The α-alumina particles (in aqueous suspension) were rotated by the magnetic field and deposited on the electrode. A multilayered, "monolithic" alumina composite of textured and equiaxed layers was thus synthesized (Fig. 25).

5.4. The EPD of fibre-reinforced, ceramic-ceramic composites

Schneider *et al.* [52] and Chawla [53] described EPD slurry infiltration followed by hot pressing, as a general way to produce of ceramic-matrix/ceramic-fibre composites (CMCs) of high density. The fabrication of

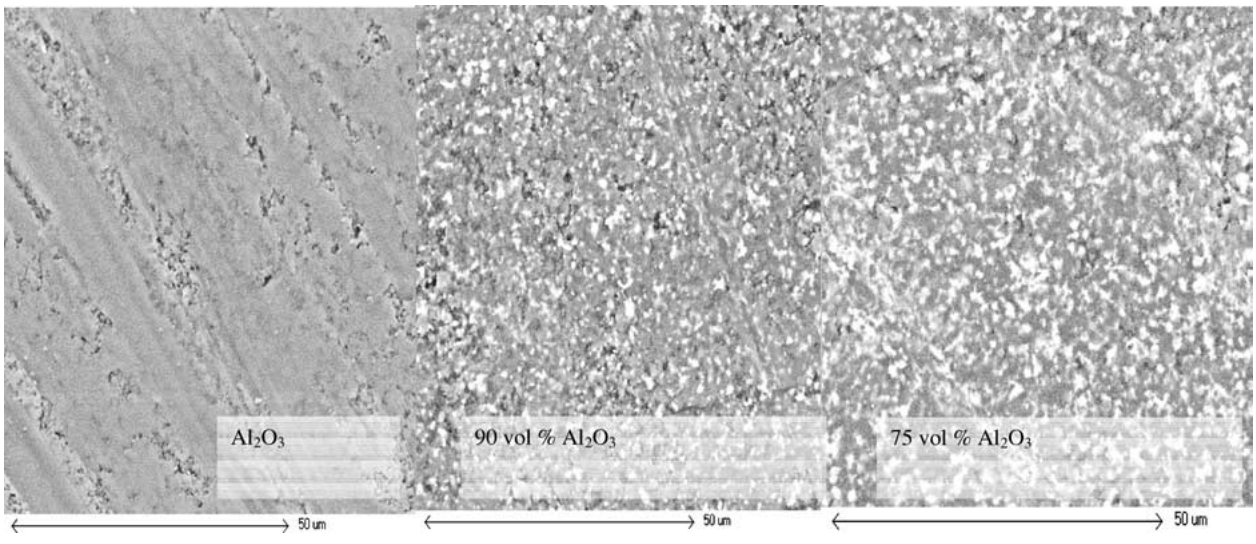

Figure 23 SEM micrographs of a Al_2O_3/Ni FGM prepared by the reduction of Al_2O_3/NiO FGM. The bright phase is Ni.

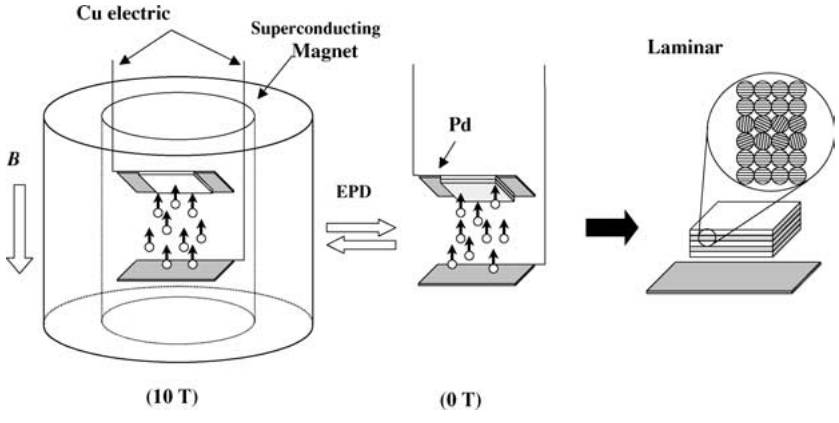

Figure 24 Laminate composite with oriented and randomly oriented layers by applying both electric and magnetic fields. (B: the applied magnetic field, Pd: Palladium substrate).

CMCs with 2-D and 3-D fibre reinforcement is difficult since complete infiltration of matrix particles into fiber tows and fabrics is resisted by microscopic openings <1 μm. Kaya *et al.* [54, 55], Westby *et al.* [56], and Kooner *et al.* [57] reported that EPD is a simple and cost-effective technique for producing fibre-reinforced CMCs but they failed to produce high-density composites. Dense composites are achievable by EPD but the fibres must be conductive, i.e., must encourage deposition, NOT infiltration. Kaya and Boccaccini [58] used stainless steel woven-fibre-mat to produce reinforced, alumina-matrix, composites of complex-shape. Westby *et al.* [56] reported infiltration of mullite into Nextel 720 fibres (Al_2O_3) using EPD. They dispersed Al_2O_3 and SiO_2 in ethanol via carboxylic acid/amine, surfactants then Nextel 720 was placed in front of the anode and the negatively-charged Al_2O_3 and SiO_2 particles infiltrated thereinto. Due to the different mobility of the particles however, the molar ratio of the deposit was different from the suspension. Kooner *et al.* [57] achieved stoichiometric deposition by controlling suspension composition but they found the deposit must be sintered $>1400^{\circ}$C for high density and high % mullite. 1400°C is above the tolerant temperature for Nextel 720 (1300°C) i.e., the tensile strength of the Nextel 720 fibres decreases at temperatures $>1300^{\circ}$C [59]. Kaya *et al.* [60, 61] infiltrated boehmite sol and colloidal silica sol (mullite precursors) into Nextel 720 at pH 4.5. A stoichiometric deposit was achieved and no cracks detected after sintering at 1200°C, but the density was $\sim$80% theoretical and the matrix was a mixture of mullite, α-Al_2O_3, and cristobalite. Kim and Nicholson [62] recently reported preparation of reaction-bonded

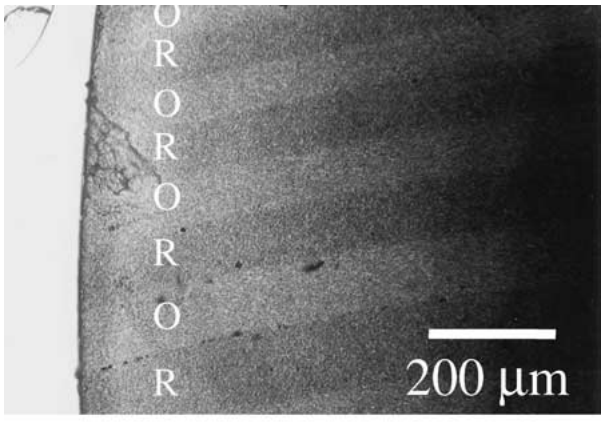

O: Oriented layer
R: Randomly-oriented layer

Figure 25 Optical micrograph of the laminar alumina composite with magnetically-oriented and randomly oriented layers.

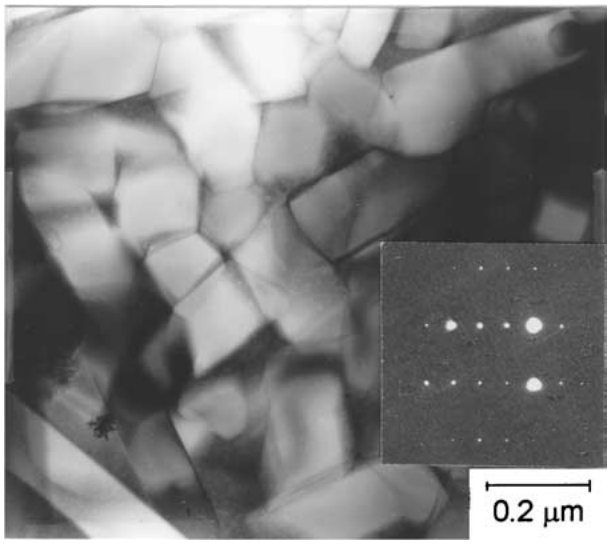

Figure 26 Transmission electron micrographs of reaction-bonded mullite matrix sintered at 1300°C for 5 h.

mullite ≤1300°C using a transient mixed-rare-earth-oxide (MREO) eutectic phase. They used Al_2O_3, Si, eutectic phase powder (Al_2O_3-SiO_2-MREO system), and mullite seeds as precursors. Silicon oxidation and mullite reaction bonding are accelerated at low temperature via the formation of a transient, low-viscosity eutectic liquid. This phase enhances diffusion compared to highly viscous, SiO_2 liquids. The eutectic liquid phase also facilitates Si oxidation and, the associated volume expansion compensates sintering shrinkage to achieve near-zero sintering shrinkage. The composition of the eutectic phase changes on reaction with the Al_2O_3 and SiO_2 to form mullite. The final sinter is >90% theoretical density, >90% mullite (by quantitative XRD) and only suffers 2.2% sintering shrinkage (Fig. 26).

Serious problems during the fabrication of continuous, ceramic-fibre-reinforced mullite composites include fibre damage and matrix cracking via sintering-induced shrinkage of the matrix; i.e., the shrinkage difference between the matrix and fibre, damages the dense fibre and the matrix that is not. The reaction-bonded-mullite-matrix protocol described matches Nextel 720 because the near-zero sintering shrinkage and low sintering temperature produces dense, high%-mullite, Nextel 720 CMC's. The Nextel 720 must however be conductive and this is achieved by the polymerisation of pyrrole on the surface thereof to polypyrrole.

6. Summary

Explanations have been aired to describe deposition during the process of EPD. It is concluded that:

(a) The coagulation of electrophoresing particles in EtOH on the oppositely charged electrode involves H^+ (H_3O^+) discharge and the accompanying pH increase moves the local suspension towards the isoelectric point of the particles.

(b) The increase of electrical resistance with time during EPD is due to the deposit and not due to the loss of current carriers from the suspension.

(c) A significant portion of the EPD-cell current is carried by the ions.

(d) The deposition electrode does not influence the process if no chemical or physical reaction is involved therewith.

(e) "Aging" occurs in non-oxide powder suspensions when TMAH is used to render the suspension basic.

(f) Evidence is presented that PEI may be a universal EPD agent for stoichiometric deposition from a mixed-powder suspension.

(g) Examples of novel-structure materials produced by EPD illustrate the unique facility of the process.

References

1. G. M. BOSE, *Phil. Trans. Roy. Soc.* **43** (1745) 419.
2. J. J. SHYNE and H. G. SCHEIBLE, "Modern Electroplating," edited by P. A. Lowenheim (John Wiley and Sons, New York, 1963) p. 714.
3. O. O. VAN DER BIEST and L. VANDEPERRE, *Ann. Rev. Mater. Sci.* **29** (1999) 327.
4. I. ZHITOMIRSKY, *Adv. in Coll. Int. Sci.* **97** (2002) 279.
5. F. GRILLION, D. FAYEULLE and M. JEANDIN, *J. Mater. Sci. Lett.* **11** (1992) 272.
6. D. R. BROWN and F. W. SALT, *J. App. Chem.* **15** (1963) 40.
7. H. KOELMAN, *Philips Res. Rep.* **10** (1955) 161.
8. P. SARKAR and P. S. NICHOLSON, *J. Amer. Ceram. Soc.* **79**(8) (1996) 1987.
9. D. DE and P. S. NICHOLSON, *ibid.* **82**(11) (1999) 3031.
10. H. C. HAMAKER and E. J. W. VERWEY, *Trans. Faraday Soc.* **36** (1940) 180.
11. L. VANDERPERRE, Ph.D. thesis, Katholieke University, Leuven, Belgium, 1998.
12. P. SARKAR, X. HUANG and P. S. NICHOLSON, *Ceram. Eng. Sci. Proc.* **14** (1993) 707.
13. J. ZHANG and B. I. LEE, *J. Amer. Ceram. Soc.* **83**(10) (2000) 2417.
14. R. MORENO and B. FERRARI, *Mater. Res. Bull.* **35** (2000) 887.
15. F. TANG, T. UCHIKOSHI, K. OZAWA and Y. SAKKA, *ibid.* **37** (2002) 653.
16. T. UCHIKOSHI, in Proc. V. Meeting on Electrophoretic Deposition for Ceramics, Japan (2001) p. 17.
17. A. J. ALDYKIEWICZ, JR., A. J. DAVENPORT and H. S. ISAACS, *J. Electrochem. Soc.* **143** (1996) 1.
18. T. UCHIKOSHI, K. OZAWA, B. D. HATTON and Y. SAKKA, *J. Mater. Res.* **16** (2001) 2.
19. P. M. BIESHEUVEL and H. VERWEIJ, *J. Amer. Ceram. Soc.* 82(6) (1999) 1451.
20. E. DE BEER, J. DUVAL and E. A. MEULENKAMP, *J. Coll. Int. Sci.* **222** (2000) 117.
21. N. YAMADA, H. SHOJI, Y. KUBO and S. KATAYAMA, *J. Mater. Sci.* **37** (2002) 2071.
22. G. WANG, P. SARKAR and P. S. NICHOLSON, *J. Amer. Ceram. Soc.* **82**(4) (1999) 849.
23. G. WANG and P. S. NICHOLSON, *ibid.* **84**(6) (2001) 1250.
24. *Idem.*, *ibid.* **80**(4) (1997) 965.
25. *Idem.*, *ibid.* **84**(9) (2001) 1977.
26. Y. FUKADA and P. S. NICHOLSON, *J. Mater. Res.* **18**(1) (2003) 2945.
27. R. J. HUNTER, "Introduction to Modern Colloid Science (Oxford Science Publications, p. 1992).
28. L. BERGSTRÖM and E. BOSTEDT, *Coll. Surf.* A. **49** (1990) 183.
29. E. LAARZ, B. V. ZHMUD and L. BERGSTRÖM, *J. Amer. Ceram. Soc.* **83**(10) (2000) 2394.
30. J. WIDEGREN and L. BERGSTRÖM, *J. Euro. Ceram. Soc.* **20** (2000) 659.

31. FUKADA and P. S. NICHOLSON, *J. Amer. Ceram. Soc.* **85**(12) (2002) 45.
32. A. BORNER and R. HERBIG, *Coll. Surf.* A **159** (1999) 439.
33. A. BORNER, R. HERBIG, M. MANGLER and G. TOMANDL, *Mater. Sci. For.* **308–311** (1999) 89.
34. K. YAMASHITA, M. NAGAI and T. UMEGAKI, *J. Mater. Sci.* **32** (1997) 6661.
35. M. NAGAI, K. YAMASHITA, T. UMEGAKI and Y. TAMUKA, *J. Amer. Ceram. Soc.* **76** (1993) 253.
36. P. SARKAR, X. HUANG and P. S. NICHOLSON, *ibid.* **76** (1993) 1055.
37. B. V. DERJAGUIN, *Discuss. Faraday Soc.* **18** (1954) 85.
38. R. HOGG, T. W. HEALY and D. W. FUERSTENAU, *Trans. Faraday Soc.* **62** (1966) 1638.
39. S. N. SIDOROV, L. M. BRONSTEIN, P. M. VALETSKY, J. HARTMANN, H. COLFEN, H. SCHNABLEGGER and M. ANTONIETTI, *J. Coll. Interf. Sci.* **212** (1999) 197.
40. J. SINDEL, N. S. BELL and W. M. SIGMUND, *J. Amer. Ceram. Soc.* **82**(11) (1999) 2953.
41. C. R. DICK and G. E. HAM, *J. Macromol. Sci. Chem.* A **4**, (1970) 1301.
42. K. HASEGAWA, M. TATSUMISAGO and T. MINAMI, *J. Ceram. Soc. Jpn* **105**(7) (1997) 569.
43. A. DIETRICH and A. NEUBRAND, *ibid.* **84**(4) (2001) 806.
44. F. TANG, T. UCHIKOSHI and Y. SAKKA, *ibid.* **85**(9) (2002) 2161.
45. T. UCHIKOSHI, T. HISASHIGE and Y. SAKKA, *J. Ceram. Soc. Jpn* **110**(9) (2002) 840.
46. H. A. KETELSON, R. PELTON and M. A. BROOK, *J. Coll. Interf. Sci.* **179** (1996) 600.
47. V. J. LARAIA and A. H. HEUER, *J. Amer. Ceram. Soc.* **72**(11) (1989) 2177.
48. M. BISSINGER, *M.S. thesis*, McMaster University, Hamilton, Canada, 1995.
49. B. HATTON and P. S. NICHOLSON, *J. Amer. Ceram. Soc.* **84**(3) (2001) 571.
50. P. SARKAR, S. DATTA and P. S. NICHOLSON, *Composites*, Part B. **28B** (1997) 49.
51. T. UCHIKOSHI, T. S. SUZUKI, H. OKUYAMA, Y. SAKKA and P. S. NICHOLSON, *J. Europ. Ceram. Soc.* in press.
52. H. SCHNEIDER, K. OKADA and J. PASK, "Mullite and Mullite Ceramics" (John Wiley & Sons, 1994).
53. K. K. CHAWLA, "Ceramic Matrix Composites" (Chapman & Hall, 1993).
54. C. KAYA, A. R. BOCCACCINI and K. K. CHAWLA, *J. Amer. Ceram. Soc.* **83** (2000) 1885.
55. C. KAYA, A. R. BOCCACCINI and P. A. TRUSTY, *J. Euro. Ceram. Soc.* **19** (1999) 2859.
56. W. S. WESTBY, S. KOONER, P. M. FARRIES, P. BOOTHER and R. A. SHATWELL, *J. Mater. Sci.* **34** (1999) 5021.
57. S. KOONER, W. S. WESTBY, C. M. A. WATSON and P. M. FARRIES, *J. Euro. Ceram. Soc.* **20** (2000) 631.
58. C. KAYA and A. R. BOCCACCINI, *J. Mater. Sci. Lett.* **20** (2001) 1465.
59. M. D. PETRY and T. MAH, *J. Amer. Ceram. Soc.* **82**(10) (1999) 2801.
60. C. KAYA, P. A. TRUSTY and C. B. PONTON, *British Ceram. Trans.* **97** (1998) 48.
61. C. KAYA, X. GU, I. AL-DAWERY and E. G. BUTLER, *Sci. Tech. Adv. Mat.* **3** (2002) 35.
62. H. S. KIM and P. S. NICHOLSON, *J. Amer. Ceram. Soc.* **85** (2002) 1730.

Received 18 December 2002
and accepted 23 July 2003